Random phase approximation effects in the longitudinal response function of ^{12}C

F. A. Brieva* and A. Dellafiore†
Swiss Institute for Nuclear Research, 5234 Villigen, Switzerland
(Received 29 December 1986)

The total photoabsorption cross section of ^{12}C and the longitudinal response function in the range of momentum transfers from 200 to 500 MeV/c are evaluated in the random-phase approximation. The random-phase-approximation polarization propagator is calculated by generalizing the doorway-state method previously developed for the Tamm-Dancoff approximation. The random-phase-approximation result is compared to the Tamm-Dancoff approximation and to experiment. The random-phase-approximation correlations cannot resolve the problem of missing strength in the quasielastic region in the range of momentum transfers between 300 and 500 MeV/c. At lower momentum transfer (200 MeV/c), as well as for photoabsorption, very good agreement with experiment can be obtained, provided other many-body effects are also taken into account. In our approach these other effects are accounted for by the imaginary part of the surface optical potential and by the width of the deeply bound hole states.

I. INTRODUCTION

The nuclear response functions measure the "willingness" of a nucleus to absorb an energy ω together with a momentum q from a given external probe. They can be studied experimentally in a variety of reactions (γ absorption, electron scattering, pion scattering, etc.). Typically, at fixed q and for increasing ω, they display narrow peaks corresponding to the excitation of low-energy discrete levels, wider peaks due to giant resonances in the continuum, and, if q is large enough, the quasielastic peak which reveals the presence, inside complex nuclei, of nucleons with properties similar to the free ones.

This picture is further complicated by the possibility that the external probe couples to the mesonic field (exchange currents) or to the internal degrees of freedom of nucleons (Δ resonance, etc.). We limit the following discussion to situations where these last processes do not play an important role. Even so, the resulting picture is still quite complex since the excitation processes mentioned above have different weights, depending on the momentum transfer q.

At a qualitative level, a single-particle model in which the nucleon struck by the external probe moves in a given mean field of finite depth and extension is able to reproduce all the features of the excitation spectrum mentioned above (discrete states, giant resonances, quasielastic peak). At a more quantitative level this simple picture needs corrections. For example, it is well known from nucleon-nucleus scattering experiments that the mean field is complex, nonlocal, and energy dependent. In Ref. 1 all these features of the phenomenological optical potential were taken into account in the calculation of inclusive electron scattering cross sections in the quasielastic regime ($q \approx 2p_F$, where p_F is the Fermi momentum).

From the point of view of many-body theory, the calculation of Ref. 1 amounts to including self-energy–type corrections to the particle propagator. At lower values of energy and momentum transfer particle-hole rescattering, which can be treated either in the Tamm-Dancoff (TDA) or in the random-phase (RPA) approximation, is known to become more and more important, especially for giant resonances and for low-lying collective states. However, at the quasielastic peak the self-energy insertions accounted for in Ref. 1 are commonly believed to give the most important many-body correction to the single-particle picture.

Indeed, the calculations of Ref. 1 gave excellent agreement with data for the scattering of 500 MeV electrons at 60° in several nuclei. It was therefore rather surprising that the model of Ref. 1, like other less sophisticated single-particle models, could not reproduce the separated longitudinal and transverse electron scattering cross sections[2] in ^{12}C and ^{40}Ca in the region of momentum transfer between 400 and 500 MeV/c.[3] Typically, the model overestimates the longitudinal response function, while underestimating the transverse one. The disagreement with the longitudinal cross section is particularly puzzling since, contrary to the transverse response, this quantity should not be affected by meson exchange currents nor by virtual isobar excitation processes.

Motivated by this disagreement, in Ref. 3 an investigation of the possible role of p-h rescattering at the kinematics of the quasielastic peak was undertaken. Calculations for a p-h force of finite range were performed in the framework of a Green's function formulation of the TDA. The ensuing integral equation for the p-h polarization propagator was solved by means of a doorway-state expansion. This method, which results in a continued-fraction expansion of the polarization propagator, is very powerful and allows for a unified description of both the discrete and continuous parts of the excitation spectrum on an equal footing. Also, residual interactions of finite range, as well as effective zero-range ones, can easily be handled with this technique.

Within the framework of the TDA, the conclusion was reached in Ref. 3 that p-h rescattering plays an important role in shifting strength from the quasielastic region into

the region of giant resonances and low-lying isoscalar collective levels for momentum transfer up to 200–300 MeV/c. The calculated response function was in good agreement with data at $q=200$ MeV/c, with some discrepancies arising already at $q=300$ MeV/c. At larger momentum transfer ($q=400-500$ MeV/c) the disagreement between the single-particle model and the Saclay data could not be attributed to p-h rescattering. It was stressed in Ref. 3 that the main problem lies in reproducing the experimental integrated cross section.

In a self-consistent calculation employing a zero-range effective interaction of the Skyrme type, Cavinato *et al.*[4] had reached different conclusions, i.e., that the data at $q=400-500$ MeV/c are well reproduced if the RPA correlations are taken into account. In Ref. 3 the result of Ref. 4 was attributed to a somewhat pathological behavior of the Skyrme interaction at large momentum transfer. However, on the basis of the calculations of Ref. 3, the possible relevance of more complicated many-body processes which are included in the RPA but not in the TDA could not be ruled out completely.

More recently, Stroth *et al.*[5] have performed RPA calculations of the longitudinal response function based on a semiclassical approximation to the underlying single-particle model. For ^{12}C they reach the conclusion that, by a careful choice of the residual interaction, the calculated response can be brought to agree with experiment near the maximum of the quasielastic peak at $q=300$ MeV/c. However, it is clear from their results that the problem of the integrated strength remains unsolved. In fact, in their calculation the transition strength is shifted by the interaction to the region of $\omega\approx 100-150$ MeV, where it overestimates experimental points, and also at $\omega\lesssim 20$ MeV, below the threshold for particle emission (in their approximation the discrete part of the excitation spectrum is treated as a continuum). Consequently, one might still wonder what would happen in a more realistic fully quantum RPA calculation which properly takes into account the finite nuclear size, like that initiated in Ref. 3.

Here we extend to the RPA the method which was developed in Ref. 3 for the TDA. This extension turns out to be relatively simple and the resulting formalism allows us to evaluate the nuclear response both for discrete states and the continuum in the framework of the RPA with a finite-range residual interaction.

We refer the reader to Refs. 1 and 3 for a detailed description of the single-particle model and of the residual interaction employed; here we merely recall the main features of our calculation:

(a) A correct treatment of the continuum as well as discrete excited states.

(b) A phenomenological account of self-energy effects through the optical potential model.

(c) A correct account of the finite range of the residual interaction.

It has been shown already in Ref. 3 that all these points are essential for a correct understanding of the role played by the residual interaction in the nuclear response function at intermediate values of energy and momentum transfer.

A desirable requirement for any model of the response function is that it should work reasonably well in the low energy and momentum-transfer region, which has been thoroughly studied both theoretically and experimentally with different techniques. For this reason we check our theory against the photoabsorption cross section, which is the long-wavelength limit of the isovector part of the longitudinal response function, and also against the low-lying discrete isoscalar excitations, whose collective character is well known. This low-energy constraint will make any eventual agreement or disagreement between our calculations and the electron scattering data at larger momentum transfer more meaningful.

II. THE DOORWAY-STATE METHOD FOR THE RPA

In this section we show how the doorway-state formalism, which was developed in Ref. 3 for the Tamm-Dancoff approximation, can be extended to the random-phase approximation.

Within the Green's function formulation of the problem, we can go from the TDA to the RPA simply by taking into account the advanced part of the polarization propagator (see, e.g., Ref. 6, p. 565). This advanced part is neglected in the TDA, while it is included in the RPA. Hence now we have, with obvious notation,

$$\Pi^0_{\mathrm{RPA}}=\Pi^0_R+\Pi^0_A\ , \tag{2.1}$$

while in Ref. 3 we had

$$\Pi^0_{\mathrm{TDA}}=\Pi^0_R\ . \tag{2.2}$$

In order to extend the doorway-state method to the RPA, we recall that in Ref. 3 the two starting doorway states $\langle D^0|$ and $|\tilde{D}^0\rangle$ were defined in such a way that

$$\Pi^0_R(q,\omega)=N^0\tilde{N}^0\langle D^0|\tilde{D}^0\rangle\ , \tag{2.3a}$$

or

$$\Pi^0_R(q,\omega)=N^0\tilde{N}^0 \tag{2.3b}$$

since

$$\langle D^0|\tilde{D}^0\rangle=1\ .$$

This means that the unperturbed propagator was given by the (properly normalized) scalar product of the first two doorway states. Equation (2.1) suggests that in order to generalize the procedure to include the advanced part of the polarization propagator, we should consider two-dimensional doorway states, say

$$\langle D^0|=(\langle D^0_+|\,,\langle D^0_-|\,) \tag{2.4a}$$

and

$$|\tilde{D}^0\rangle=\begin{pmatrix}|\tilde{D}^0_+\rangle\\ |\tilde{D}^0_-\rangle\end{pmatrix} \tag{2.4b}$$

such that

$$\Pi^0_R(q,\omega)+\Pi^0_A(q,\omega)$$
$$=(N^0\tilde{N}^0)_{\mathrm{RPA}}(\langle D^0_+|\tilde{D}^0_+\rangle+\langle D^0_-|\tilde{D}^0_-\rangle)\ , \tag{2.5a}$$

with the normalization condition

$$\langle D^0 \mid \tilde{D}^0 \rangle = \langle D^0_+ \mid \tilde{D}^0_+ \rangle + \langle D^0_- \mid \tilde{D}^0_- \rangle = 1 \ . \tag{2.5b}$$

The term $\langle D^0_+ \mid \tilde{D}^0_+ \rangle$ will be proportional to the retarded part Π^0_R of the polarization propagator, while the term $\langle D^0_- \mid \tilde{D}^0_- \rangle$ will be proportional to the advanced part Π^0_A. To prove this statement, we write down the explicit expressions needed for calculating the nuclear response to an external operator $O(q)$ (in order to avoid unnecessary complications here we omit c.m. corrections; they will be included in the Appendix):

$$\Pi^0_R(q,\omega) = \sum_{i\alpha} \int d\mathbf{r}_1 d\mathbf{r}_2 \phi^\dagger_i(\mathbf{r}_2) O^\dagger(2) \phi_\alpha(\mathbf{r}_2) \frac{\theta(\alpha - F)\theta(F - i)}{\omega - \epsilon_{\alpha i} + i\eta} \times \phi^\dagger_\alpha(\mathbf{r}_1) O(1) \phi_i(\mathbf{r}_1) \tag{2.6a}$$

and

$$\Pi^0_A(q,\omega) = \sum_{i\alpha} \int d\mathbf{r}_1 d\mathbf{r}_2 \phi^\dagger_\alpha(\mathbf{r}_2) O^\dagger(2) \phi_i(\mathbf{r}_2) \frac{\theta(\alpha - F)\theta(F - i)}{-\omega - \epsilon_{\alpha i} + i\eta} \times \phi^\dagger_i(\mathbf{r}_1) O(1) \phi_\alpha(\mathbf{r}_1) \ . \tag{2.6b}$$

In these equations the index α runs over all the single-particle states above the Fermi level F, while the sum over i is limited to the occupied states. An essential step in the calculation of Π^0 requires expressing the infinite sum over α in terms of a single-particle Green's function

$$G(\mathbf{r}_2, \mathbf{r}_1, \omega - \mid \epsilon_i \mid) = \sum_\alpha \phi_\alpha(\mathbf{r}_2) \frac{1}{\omega - \mid \epsilon_i \mid - \epsilon_\alpha + i\eta} \phi^\dagger_\alpha(\mathbf{r}_1) - \sum_j \theta(F - j) \phi_j(\mathbf{r}_2) \frac{1}{\omega - \epsilon_{ji} + i\eta} \phi^\dagger_j(\mathbf{r}_1) . \tag{2.7}$$

The first term on the right-hand side can be easily evaluated as the product of regular times irregular solutions of the Schrödinger equation.[7] This automatically takes care of the sum over the infinite set $\{\alpha\}$ and we are left only with the finite sum over the occupied states j. The same method can be extended to evaluate the Green's function of particles propagating in a complex optical potential.[1]

$$\Pi^0_R(q,\omega) = \sum_i \theta(F - i) \int d\mathbf{r}_1 d\mathbf{r}_2 \phi^\dagger_i(\mathbf{r}_2) O^\dagger(2) \times G(\mathbf{r}_2, \mathbf{r}_1, \omega - \mid \epsilon_i \mid) O(1) \phi_i(\mathbf{r}_1) \tag{2.8a}$$

and

$$\Pi^0_A(q,\omega) = \sum_i \theta(F - i) \times \int d\mathbf{r}_1 d\mathbf{r}_2 \phi^\dagger_i(\mathbf{r}_1) O(1) \times G(\mathbf{r}_1, \mathbf{r}_2, -\omega - \mid \epsilon_i \mid) O^\dagger(2) \phi_i(\mathbf{r}_2) \ . \tag{2.8b}$$

Now, in analogy with Eqs. (3.8) of Ref. 3, we define

$$N^0 \langle D^0_+ \mid \mathbf{r}_2 \rangle = \sum_j \phi^\dagger_j(\mathbf{r}_2) O^\dagger(2) \langle j^{-1} \mid \tag{2.9a}$$

and

$$N^0 \langle \mathbf{r}_2 \mid \tilde{D}^0_+ \rangle = \sum_i \mid i^{-1} \rangle \int d\mathbf{r}_1 G(\mathbf{r}_2, \mathbf{r}_1, \omega - \mid \epsilon_i \mid) \times O(1) \phi_i(\mathbf{r}_1) \ , \tag{2.9b}$$

so that

$$\Pi^0_R(q,\omega) = N^0 \tilde{N}^0 \int d\mathbf{r}_2 \langle D^0_+ \mid \mathbf{r}_2 \rangle \langle \mathbf{r}_2 \mid \tilde{D}^0_+ \rangle = N^0 \tilde{N}^0 \langle D^0_+ \mid \tilde{D}^0_+ \rangle \ . \tag{2.10a}$$

In order to get Eq. (2.5a) for the full propagator Π^0, we would also like to write Π^0_A in the form

$$\Pi^0_A(q,\omega) = N^0 \tilde{N}^0 \langle D^0_- \mid \tilde{D}^0_- \rangle \ . \tag{2.10b}$$

However, a small complication arises because of the different spin-isospin structure in expressions (2.8a) and (2.8b). If, in analogy with Eqs. (2.9), we define

$$N^0 \langle D^0_- \mid \mathbf{r}_2 \rangle = \sum_j O^\dagger(2) \phi_j(\mathbf{r}_2) \mid j^{-1} \rangle \tag{2.11a}$$

and

$$N^0 \langle \mathbf{r}_2 \mid \tilde{D}^0_- \rangle = \sum_i \langle i^{-1} \mid \int d\mathbf{r}_1 \phi^\dagger_i(\mathbf{r}_1) O(1) \times G(\mathbf{r}_1, \mathbf{r}_2, -\omega - \mid \epsilon_i \mid) \ , \tag{2.11b}$$

Eq. (2.8b) becomes

$$\Pi^0_A(q,\omega) = N^0 \tilde{N}^0 \int d\mathbf{r}_2 \langle \mathbf{r}_2 \mid \tilde{D}^0_- \rangle \langle D^0_- \mid \mathbf{r}_2 \rangle \ , \tag{2.12}$$

i.e., we get a slightly unusual definition for the scalar product in (2.10b):

$$\langle D^0_- \mid \tilde{D}^0_- \rangle = \int d\mathbf{r}_2 \langle \mathbf{r}_2 \mid \tilde{D}^0_- \rangle \langle D^0_- \mid \mathbf{r}_2 \rangle \ . \tag{2.13}$$

This is not an essential difficulty; the more standard definition (2.10a) for the r representation of the scalar product of the states $\langle D^0_- \mid$ and $\mid \tilde{D}^0_- \rangle$ could be obtained if we were willing to separate the spin-isospin coordinates from the spatial coordinates in Eq. (2.8b). However, since this would result in a more complicated notation, we stick to the definition (2.13).

Thus we have given the explicit expression of the doorway states (2.4) needed to calculate the polarization propagator Π^0, including both the retarded and advanced part. Apart from the normalization, the initial doorway states in the TDA calculation of Ref. 3 correspond to $\langle D^0_+ \mid$ and $\mid \tilde{D}^0_+ \rangle$, while the two additional "small" components $\langle D^0_- \mid$ and $\langle \tilde{D}^0_- \mid$ appear only in the RPA.

In Ref. 3 the higher-order doorway states were generated by repeated application of an operator $\hat{\Omega}^0$ to the initial doorway states. The explicit form of $\hat{\Omega}^0$ could be deduced from the first order correction to Π^0. Clearly, the same approach can be followed in the RPA and the re-

currence relations (3.10) of Ref. 3 can be used to generate the higher order doorway states. However, now, because of the two-dimensional structure of the RPA doorway states (2.4), the operator $\hat{\Omega}^0$ becomes a 2×2 matrix acting in the doorway-state space. If we define

$$\hat{\Omega}^0=\begin{bmatrix}\hat{W} & \hat{X}\\ \hat{Y} & \hat{Z}\end{bmatrix}, \tag{2.14}$$

the matrix elements of $\hat{\Omega}^0$ between two generic RPA doorway states become

$$\Omega^0_{jk}=\langle D^j_+ \mid \hat{W} \mid \tilde{D}^k_+\rangle+\langle D^j_+ \mid \hat{X} \mid \tilde{D}^k_-\rangle +\langle D^j_- \mid \hat{Y} \mid \tilde{D}^k_+\rangle+\langle D^j_- \mid \hat{Z} \mid \tilde{D}^k_-\rangle . \tag{2.15}$$

The matrix element of $\hat{W}$ corresponds (except for the normalization) to the TDA term in Eq. (3.11b) of Ref. 3, while the additional terms in Eq. (2.15) are the RPA corrections.

In complete analogy with Eq. (3.11a) of Ref. 3, we can write a continued-fraction expansion for the polarization propagator in the random phase approximation,

$$\Pi(q,\omega)_{\rm RPA}=\frac{\Pi^0(q,\omega)_{\rm RPA}}{1-\Omega^0_{00}-\dfrac{\Omega^0_{01}\Omega^0_{10}}{1-\Omega^0_{11}-\cdots}} . \tag{2.16}$$

Neglect of the advanced part of Π^0 in the numerator and of the $\hat{X}$, $\hat{Y}$, and $\hat{Z}$ terms in the matrix elements (2.15) reproduces the TDA result of Ref. 3.

It is worth stressing that the doorway-state method gives the same structure for the expansion of the polarization propagator both in the TDA and the RPA. Actually, the method is quite general and to a large extent it is not affected by the details of the dynamical problem to which it is applied.

Proceeding as in Ref. 3, we can obtain the coordinate representation of the operator $\hat{\Omega}^0$ by writing down the first-order correction to the single-particle polarization propagator and by separating out the zero-order doorway states. We get

$$\langle \mathbf{r}_2 \mid \hat{W} \mid \mathbf{r}_4\rangle=\sum_{ij} \mid j^{-1}\rangle \int d\mathbf{r}_3[G(\mathbf{r}_2,\mathbf{r}_3,\omega- \mid \epsilon_j \mid)\phi^\dagger_i(\mathbf{r}_4)-G(\mathbf{r}_2,\mathbf{r}_4,\omega- \mid \epsilon_j \mid)\phi^\dagger_i(\mathbf{r}_3)]V(\mathbf{r}_3,\mathbf{r}_4)\phi_j(\mathbf{r}_3)\langle i^{-1}\mid , \tag{2.17a}$$

$$\langle \mathbf{r}_2 \mid \hat{X} \mid \mathbf{r}_4\rangle=\sum_{ij} \mid j^{-1}\rangle \int d\mathbf{r}_3 G(\mathbf{r}_2,\mathbf{r}_3,\omega- \mid \epsilon_j \mid)V(\mathbf{r}_3,\mathbf{r}_4)[\phi_j(\mathbf{r}_3)\phi_i(\mathbf{r}_4)-\phi_j(\mathbf{r}_4)\phi_i(\mathbf{r}_3)]\langle i^{-1}\mid , \tag{2.17b}$$

$$\langle \mathbf{r}_2 \mid \hat{Y} \mid \mathbf{r}_4\rangle=\sum_{ij} \mid j^{-1}\rangle \int d\mathbf{r}_3[\phi^\dagger_j(\mathbf{r}_3)\phi^\dagger_i(\mathbf{r}_4)-\phi^\dagger_j(\mathbf{r}_4)\phi^\dagger_i(\mathbf{r}_3)]V(\mathbf{r}_3,\mathbf{r}_4)G(\mathbf{r}_3,\mathbf{r}_2,-\omega- \mid \epsilon_j \mid)\langle i^{-1}\mid , \tag{2.17c}$$

$$\langle \mathbf{r}_2 \mid \hat{Z} \mid \mathbf{r}_4\rangle=\sum_{ij} \mid j^{-1}\rangle \int d\mathbf{r}_3\phi^\dagger_i(\mathbf{r}_3)V(\mathbf{r}_3,\mathbf{r}_4)[G(\mathbf{r}_3,\mathbf{r}_2,-\omega- \mid \epsilon_j \mid)\phi_i(\mathbf{r}_4)-\phi_i(\mathbf{r}_3)G(\mathbf{r}_4,\mathbf{r}_2,-\omega- \mid \epsilon_j \mid)]\langle i^{-1}\mid , \tag{2.17d}$$

and

$$\langle D^j_+ \mid \hat{W} \mid \tilde{D}^k_+\rangle=\int d\mathbf{r}_2\, d\mathbf{r}_4\langle D^j_+ \mid \mathbf{r}_2\rangle \times\langle \mathbf{r}_2 \mid \hat{W} \mid \mathbf{r}_4\rangle\langle \mathbf{r}_4 \mid \tilde{D}^k_+\rangle , \tag{2.18a}$$

$$\langle D^j_+ \mid \hat{X} \mid \tilde{D}^k_-\rangle=\int d\mathbf{r}_2\, d\mathbf{r}_4\langle D^j_+ \mid \mathbf{r}_2\rangle \times\langle \mathbf{r}_4 \mid \tilde{D}^k_-\rangle\langle \mathbf{r}_2 \mid \hat{X} \mid \mathbf{r}_4\rangle , \tag{2.18b}$$

$$\langle D^j_- \mid \hat{Y} \mid \tilde{D}^k_+\rangle=\int d\mathbf{r}_2\, d\mathbf{r}_4\langle \mathbf{r}_2 \mid \hat{Y} \mid \mathbf{r}_4\rangle \times\langle D^j_- \mid \mathbf{r}_2\rangle\langle \mathbf{r}_4 \mid \tilde{D}^k_+\rangle , \tag{2.18c}$$

$$\langle D^j_- \mid \hat{Z} \mid \tilde{D}^k_-\rangle=\int d\mathbf{r}_2\, d\mathbf{r}_4\langle \mathbf{r}_4 \mid \tilde{D}^k_-\rangle \times\langle \mathbf{r}_2 \mid \hat{Z} \mid \mathbf{r}_4\rangle\langle \mathbf{r}_2 \mid D^j_-\rangle . \tag{2.18d}$$

Note the order of the various terms in the last three equations. As in Eq. (2.13), every time we have either a D_- or a $\tilde{D}_-$, we need to exchange the order of terms in the scalar product.

As in the TDA case, in order to evaluate explicitly the continued fraction (2.16), we make a partial-wave decomposition of the various quantities needed and obtain a continued fraction expansion for each partial-wave component of the polarization propagator which can then be easily evaluated numerically. Details are given in the Appendix.

III. NUCLEAR MATTER ESTIMATES

Here we discuss the effects of particle-hole rescattering in the quasielastic peak region, by using simple nuclear matter arguments.

In Ref. 3 an estimate of the effect of the residual interaction in the TDA was obtained by looking at the first-order correction to the nuclear-matter polarization propagator

$$\Pi^{(1)}=\Pi^0+\Pi^0\tilde{V}_\alpha\Pi^0 . \tag{3.1}$$

The residual interaction $\tilde{V}_\alpha$, given by Eqs. (4.10) of Ref. 3, depends on the isospin channel, so that the particle-hole rescattering has different effects on the isoscalar and isovector response. The results obtained in Ref. 3 for a real residual interaction can be summarized as follows, for the TDA,

$$(\delta\omega)_{\rm TDA}=\tfrac{3}{2}\rho_0\tilde{V}_\alpha+\mathcal{O}(V^2_\alpha) , \tag{3.2a}$$

$$\frac{{\rm Im}\Pi^{(1)}}{{\rm Im}\Pi^0}=1+\mathcal{O}(V^2_\alpha) . \tag{3.2b}$$

At first order the residual interaction shifts the peak position by an amount $\delta\omega$, which is proportional to the value of the residual interaction in that particular isospin channel and to the nuclear matter density,

$$\rho_0=\tfrac{2}{3}p^3_F/\pi^2 .$$

Since $\tilde{V}_\alpha$ has opposite signs in the isoscalar and isovector channels, the shift occurs in opposite directions for the two isospin components of the longitudinal response. Always at first order in $\tilde{V}_\alpha$, the value of the response function at the maximum is not affected by the residual interaction [Eq. (3.2b)]. This fact is a consequence of the vanishing of the real part of $\Pi^0_{\rm TDA}$ at the quasielastic peak. The results (3.2) are in qualitative agreement with the well known property of the TDA of preserving the non-energy-weighted sum rule (NEWSR), while violating the energy-weighted one (EWSR).

In the RPA the real part of Π^0 no longer vanishes at the quasielastic peak because of the tail of the advanced part Π^0_A. Thus we expect that Eq. (3.2b) will not hold in RPA.

In order to make more quantitative statements, we take an expansion of $\Pi^0(q,\omega)$ near the quasielastic peak, analogous to Eq. (4.3) of Ref. 3. However, now we include also the advanced part of the polarization propagator. For momentum transfer $q \geq 2p_F$,

$$\Pi^0(q,\omega)=\frac{1}{4}\frac{\rho_0}{q^2/2m}\left\{-1+\frac{1}{2}\left[\frac{1}{q^2/2m}+\frac{3}{p_F^2/2m}\right]\omega_q-\frac{1}{4}\frac{\omega_q^2}{q^2/2m}-i\pi\frac{3}{4}\frac{q}{p_F}\left[1-\frac{1}{4}\frac{\omega_q^2}{(q^2/2m)(p_F^2/2m)}\right]\right\}+\mathcal{O}(\omega_q^3)\ . \tag{3.3}$$

We have retained all terms up to second order in

$$\omega_q=\omega-q^2/2m\ .$$

By inserting (3.3) into (3.1), and keeping terms up to ω_q^2, we easily obtain, for the RPA,

$$(\delta\omega)_{\rm RPA}\approx\tfrac{3}{2}\rho_0\tilde{V}_\alpha\left[1+\frac{1}{3}\frac{p_F^2}{q^2}\right]\approx(\delta\omega)_{\rm TDA}\ , \tag{3.4a}$$

$$\frac{{\rm Im}\Pi^{(1)}}{{\rm Im}\Pi^0}\approx 1-\frac{1}{3}\frac{\delta\omega}{q^2/2m}\ . \tag{3.4b}$$

Thus, in the RPA the shift of the quasielastic peak due to the residual interaction is roughly the same as in the TDA; instead, the height of the peak is changed by an amount proportional to the shift itself. The isovector response, for which $\delta\omega$ is positive, is quenched in the RPA, while the isoscalar response is enhanced, since in this channel $\delta\omega<0$. These results are in qualitative agreement with the well known property of the RPA of preserving the EWSR while violating the NEWSR.

The effect of the residual interaction on the quasielastic peak is sketched in Fig. 1 for both the TDA and RPA. The resulting longitudinal response is also shown. In both cases the height of the longitudinal peak is decreased; however, in the TDA the longitudinal NEWSR is exactly the same as the free one, while, in the situation shown in Fig. 1, it is slightly increased in the RPA. This increase of the RPA NEWSR is due to the stronger effective residual interaction in the isoscalar channel compared to the isovector channel. The only way of obtaining a decrease in the longitudinal NEWSR with a real residual interaction would be to assume a force which is stronger in the isovector channel. Then the quenching of the isovector part would not be completely compensated for by the enhancement of the isoscalar components. However, such a force would inevitably quench also the transverse response which, at large q, is mostly isovector.

Thus our simple nuclear matter arguments show that particle-hole rescattering, evaluated either in the TDA or RPA, is unlikely to resolve the discrepancy between theory and experiment for the separated electron scattering cross sections in the quasielastic region. This statement holds for any real residual interaction of reasonable strength (a complex residual interaction would change the results obtained above).

We will see in the next section that these conclusions are confirmed by our numerical calculations for finite nuclei.

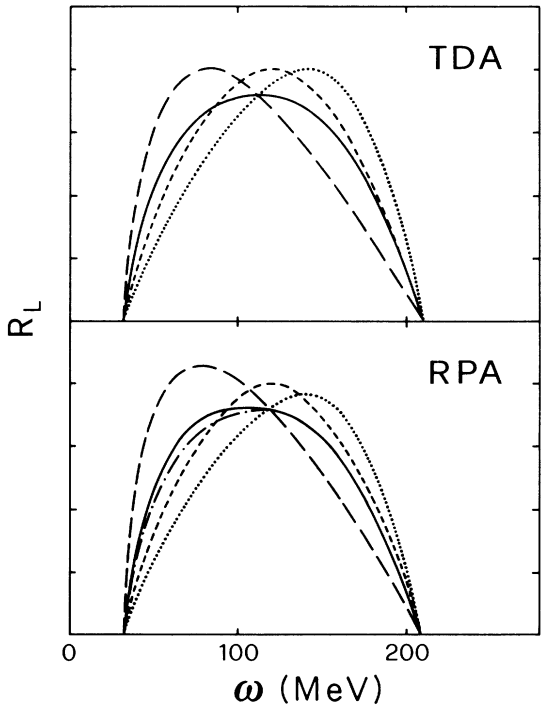

FIG. 1. Qualitative effect of residual interaction on the nuclear matter response function. The short-dashed line shows the longitudinal response without p-h interaction. The long-dashed curve is the isoscalar response evaluated either in the TDA (upper) or RPA (lower). Similarly, the dotted line gives the isovector response. The solid line in the upper part of the figure gives the longitudinal response (isoscalar plus isovector) in the TDA. In the lower part of the figure the solid line gives the RPA longitudinal response, while the dotted-dashed line is the TDA longitudinal response.

IV. RESULTS

The results of our numerical calculations for the longitudinal response function are displayed in Figs. 2–5. Both the single-particle model and the residual interactions are exactly the same as in Ref. 3; thus comparison of our present results (solid line) with the results of Ref. 3 (dashed lines) shows just the effect of the RPA correlations, which had been neglected in the TDA calculation of Ref. 3. We note that, at large q, near the maximum of the quasielastic peak, our numerical calculations agree with the nuclear matter estimates of the preceding section. Moreover, our results displayed in Figs. 2–5 are in qualitative agreement with the results of coupled-channel calculations by Balashov *et al.*[9]

The curves at $q=500$, 400, and 300 MeV/c display some common features. The RPA correlations do not improve the agreement with experiment with respect to the previous TDA results. Actually, in the RPA the discrepancy between theory and experiment is even larger than in the TDA. This is a consequence of the fact that the RPA tends to preserve the EWSR rather than the NEWSR, as discussed in the preceding section. The enhancement of the response function in the low energy region is due to the increased isoscalar response. The sharp peak just above threshold, which is mostly a $T=0$, $L=2$ resonance, is also more pronounced than in the TDA.

At $q=200$ MeV/c the TDA and RPA results in the continuum are rather similar, as shown in Fig. 5. The isoscalar quadrupole resonance just above threshold has similar strength in both approximation schemes. The same is true for the sharp peak at an intrinsic excitation energy of about 30 MeV (in Fig. 4 of Ref. 3 one point was missed and this peak was less intense; the correct result is that shown here in Fig. 5). This sharp peak, which is present also at $q=300$ MeV/c (see Fig. 4), arises in the isovector dipole channel. In order to understand better the origin of this peak, which does not seem to be reproduced by the electron scattering data, it is useful to study explicitly the photoabsorption process.

The dashed line in Fig. 6 gives the photoabsorption cross section calculated without residual interaction, i.e., in the single-particle model of Ref. 1. Clearly, the giant dipole excitation is overdamped by the imaginary part of the phenomenological optical potential employed. At these low energies of the outgoing nucleon, the imaginary optical potential is dominated by the surface term, which is of the form $W_s F(E)$, where $F(E)$ is a decreasing function of the nucleon energy.[11] In the parametrization of

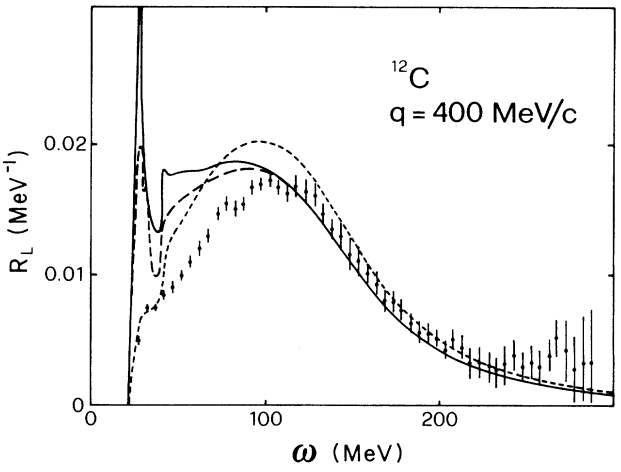

FIG. 3. Same as Fig. 2, but for $q=400$ MeV/c.

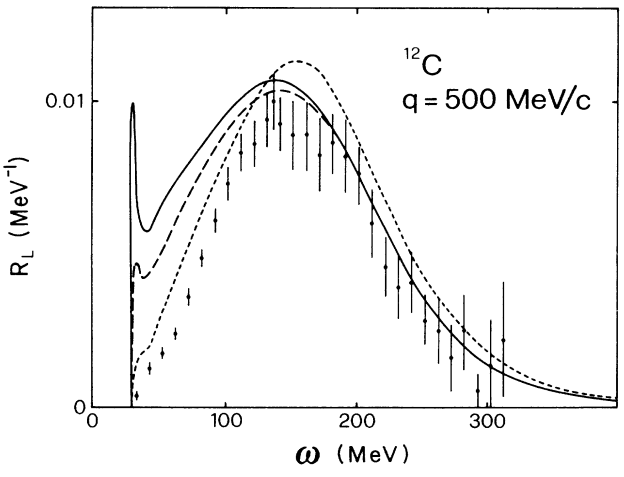

FIG. 2. Longitudinal response function at fixed $q=500$ MeV/c. The dashed curves are the results of Ref. 3 (short-dashed, single-particle response; long-dashed (TDA). The solid line includes RPA correlations. Experimental points from Ref. 8.

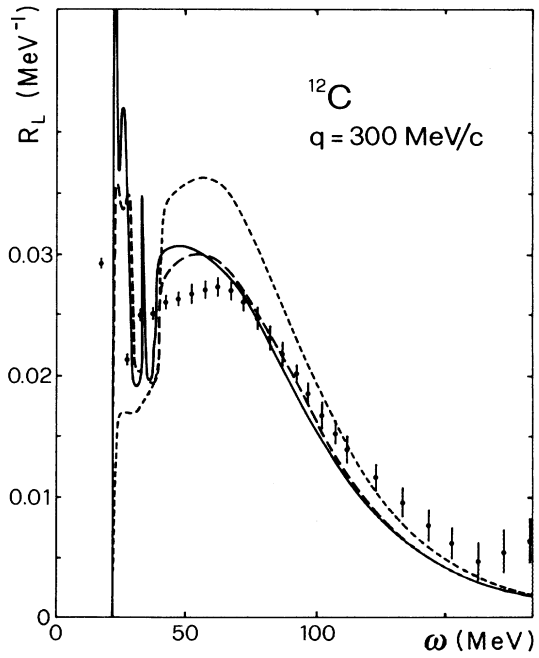

FIG. 4. Same as Fig. 2 but for $q=300$ MeV/c.

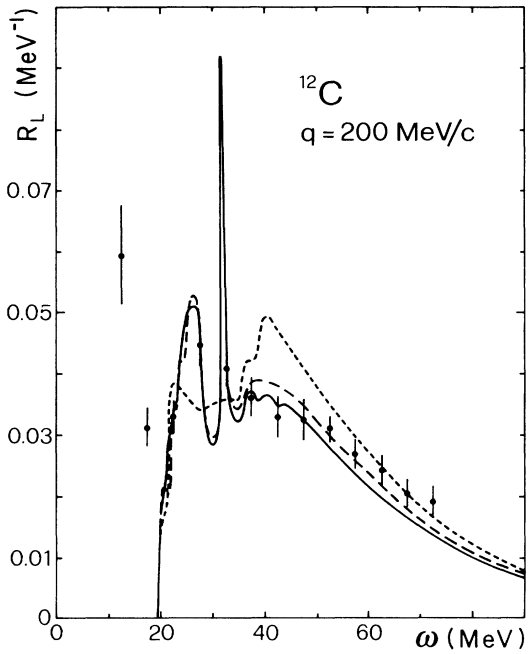

FIG. 5. Same as Fig. 2, but for $q=200$ MeV/c.

Ref. 1, $W_s=14$ MeV was taken for the imaginary surface potential. However, for very small outgoing nucleon energies, like those occurring in photoabsorption, a more appropriate value of W_s would be $W_s\approx 5$ MeV.[12] In the following we treat W_s as a free parameter, to be determined by fitting the properties of the giant dipole resonance. The solid line in Fig. 6 shows the result of setting $W_s=0$. Then, the cross section shows two well defined peaks around 20 MeV corresponding to $1p_{3/2}\rightarrow d_{5/2}$ excitations (the lowest peak is a proton excitation and the highest a neutron excitation; see also Fig. 7). Comparison of the two curves in Fig. 6 shows the strong dependence of the photoabsorption cross section on W_s.

If, always with $W_s=0$, the residual interaction is switched on, the results shown in Fig. 7 by the long-dashed (TDA) and dotted-dashed (RPA) curves are obtained. The following remarks are in order.

In the isovector channel the two approximation schemes (TDA and RPA) give very similar results. The $1p_{3/2}\rightarrow d_{5/2}$ strength is quenched and shifted by the residual interaction to about the experimental maximum of the dipole strength; however, the absolute value at the maximum remains too large by almost a factor of 2. A strong secondary peak appears at an excitation energy of about 30 MeV.

A similar two-peak structure of the photoabsorption cross section has been obtained in a continuum RPA calculation with a Skyrme force.[13] In order to understand the origin of this high-energy peak, it is useful to calculate the response without residual interaction, but giving a small imaginary part to ω. As pointed out in Ref. 3 this is a way of displaying the discrete excitations which correspond to the poles of the Green's function (here the full power of the Green's function method, which allows a simultaneous treatment of both discrete and continuous excitations, becomes apparent). The short-dashed line in Fig. 7 shows the result of such a calculation. This procedure unveils a discrete excitation at $\omega\approx 19$ MeV corre-

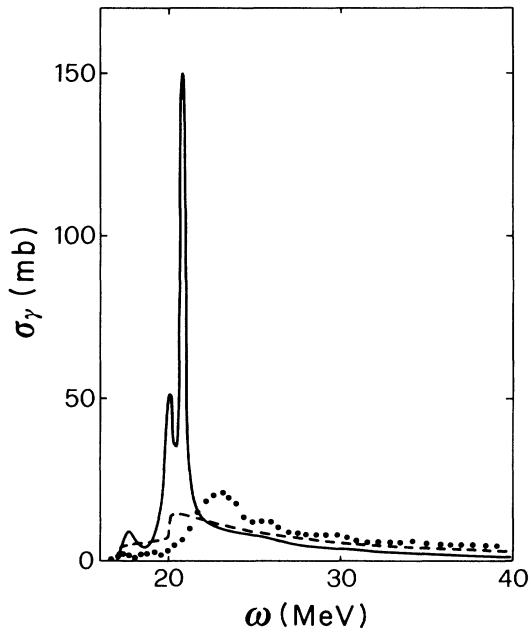

FIG. 6. Photoabsorption cross section in single-particle model with the optical potential of Ref. 1 (dashed line). The solid line is calculated in the same model, but with no surface absorption ($W_s=0$). The dots show the experimental data from Ref. 10.

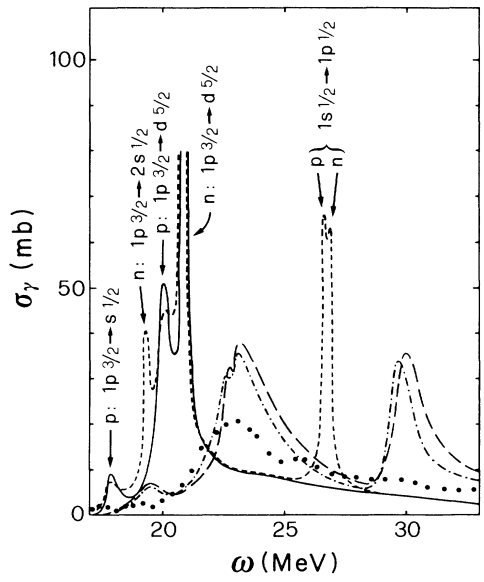

FIG. 7. Photoabsorption cross section in various approximations. The solid line is the same as in Fig. 6. The short-dashed line is obtained in the same model by giving a small imaginary part of 0.5 MeV to ω. The single-particle transitions contributing to the various peaks are shown explicitly. The long-dashed line is the result of including the residual interaction in the TDA and the dotted-dashed line in the RPA.

sponding to a neutron $1p_{3/2} \rightarrow 2s_{1/2}$ transition, which in our potential happens to be just bound, as well as a peak at $\omega \approx 27$ MeV which corresponds to excitation of the low-lying $1s_{1/2}$ nucleons to the bound $1p_{1/2}$ level. Through the residual interaction this last discrete excitation acquires a width and is shifted upwards in energy, giving rise to the strong secondary peak at $\omega \approx 30$ MeV.

If we now allow for some surface absorption in the optical potential, the strength of the main peak at $\omega \approx 23$ MeV can be brought into agreement with experiment, but the peak at 30 MeV is not affected, in agreement with our interpretation of the origin of this peak. This is displayed in Fig. 8, which shows the result of our RPA calculations with a moderate surface absorption $W_s = 5$ MeV.

The peak at 30 MeV in the RPA calculation of the photoabsorption strength arises also in our calculated longitudinal electron scattering structure function at $q = 200$ and 300 MeV/c (cf. Figs. 4 and 5). Since neither the photoabsorption nor the electron scattering data show such a pronounced peak at this energy, clearly there must be some smearing mechanism which has not been taken into account in our calculations. One possible source of smearing of this peak has been pointed out by Rowe and Wong[14] in the framework of discrete RPA calculations of the photoabsorption cross section. These authors argue that ^{12}C is not a closed $1p_{3/2}$-shell nucleus. A more realistic description of this nucleus should allow for partial occupation of the $1p_{1/2}$ shell. Clearly, this would result in a smearing of the high-energy peak since now the $1s_{1/2}$ nucleons could be excited to both the $1p_{3/2}$ and $1p_{1/2}$ levels. However, there is an additional effect which can give a spreading of this transition strength. It is well known from (ee'p) experiments[15] that the low-lying hole levels are far from well defined in energy. In particular, the $1s_{1/2}$ nucleons in ^{12}C show a spreading around the mean binding energy which can be described by a width $\Gamma_h \approx 4.5$ MeV.

We have performed our RPA calculation of the photoabsorption cross section assuming a complex energy for the $1s_{1/2}$ holes with the above imaginary part. The result is shown in Fig. 9, where the dashed line shows the optical model result (with $W_s = 5$ MeV) and the solid line includes the effect of residual interaction in the RPA. We can see that the high-energy peak has been completely washed out by the imaginary part of the $1s_{1/2}$-hole energy. The agreement of the RPA curve with experiment is quite reasonable.

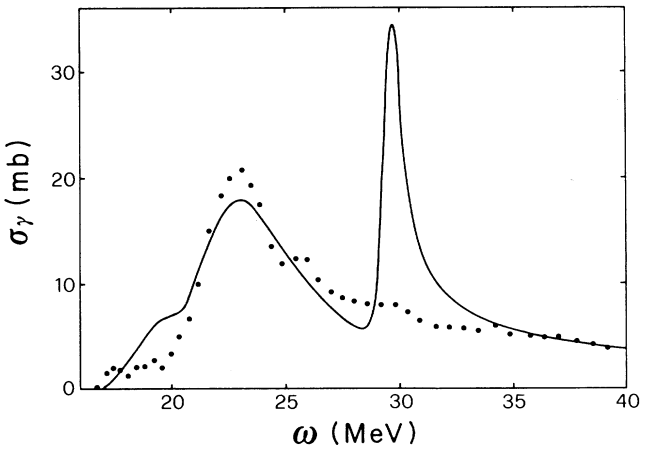

FIG. 8. Photoabsorption cross section in the RPA with the optical potential of Ref. 1, except for the imaginary surface term, which here is $W_s = 5$ MeV instead of $W_s = 14$ MeV.

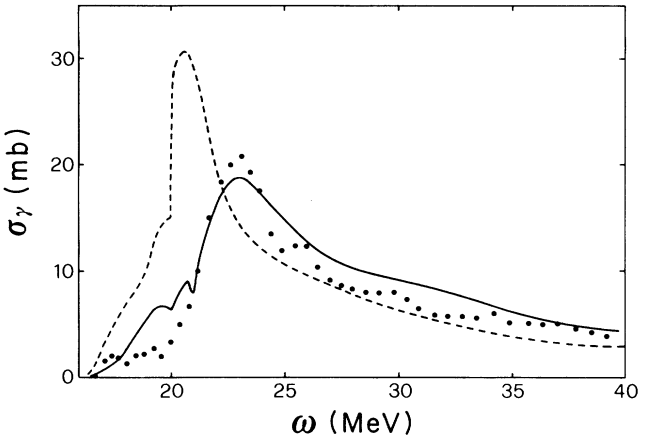

FIG. 9. The dashed line shows the photoabsorption cross section calculated in the modified optical potential of Ref. 1, with reduced surface absorption ($W_s = 5$ MeV) and complex $1s_{1/2}$ hole energy ($\Gamma_h = 4.5$ MeV). The solid line is the result of our RPA calculations. The data are from Ref. 10.

It is worth stressing that, while the role of the residual interaction is essential in shifting the strength of the $1p_{3/2} \rightarrow d_{5/2}$ transition to the experimental value at about 23 MeV, to reproduce both the strength and shape of the giant dipole resonance requires taking into account effects which go beyond the usual RPA. For example, as shown in Ref. 16, the coupling of 1p-1h to 2p-2h states redistributes the strength and wipes out unphysical bumps in the RPA isovector dipole response. This kind of effect has been included phenomenologically in our calculation through the imaginary part of the surface optical potential W_s and the width Γ_h of the hole energies for the deeply bound nucleons.

Having adjusted the parameters of the optical potential to give a good description of the photoabsorption cross section, we can go back and calculate the electron scattering resonse function. In Fig. 10 we show the result of our RPA calculation at $q = 200$ MeV/c, using the same parameters W_s and Γ_h employed to fit the photoabsorption data. The overall agreement with experiment is quite reasonable. Comparison with Fig. 5 shows that the sharp isovector dipole peak at 30 MeV excitation energy has been completely smeared out. We will comment later on the peak at $\omega \approx 12$ MeV.

The same calculation at $q = 300$ MeV/c gives the result displayed in Fig. 11. Comparison with Fig. 4 shows that the strong isoscalar quadrupole resonance around 24 MeV has been partially damped, while the sharp isovector dipole peak has completely disappeared. However, the response function in the quasielastic region ($\omega \approx 50$ MeV) is practically unchanged with respect to the calculation of Fig. 4 and remains too large compared to experiment.

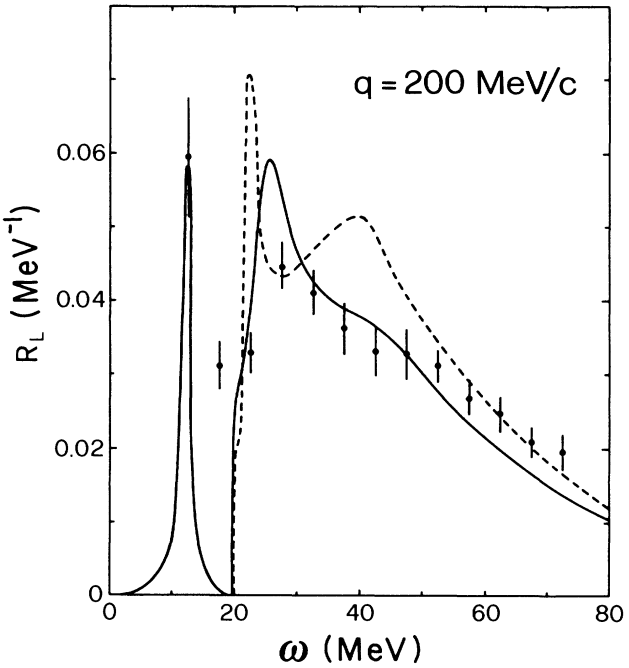

FIG. 10. Longitudinal response function at $q=200$ MeV/c. Theoretical curves are the same as in Fig. 9. Data from Ref. 8. The sharp peak at $\omega \approx 12$ MeV gives the isoscalar octupole strength calculated in the RPA. It has been obtained by adding an imaginary part of 0.5 MeV to ω. There is practically no octupole strength below threshold in the single-particle model without residual interaction.

Similarly, the new values of W_s and Γ_h would not appreciably modify the response in the quasielastic region at 400 and 500 MeV/c momentum transfer, with respect to that displayed in Figs. 2 and 3.

As mentioned above, our method can be applied also to the discrete low-lying states like the $T=0$, $L=2$, and

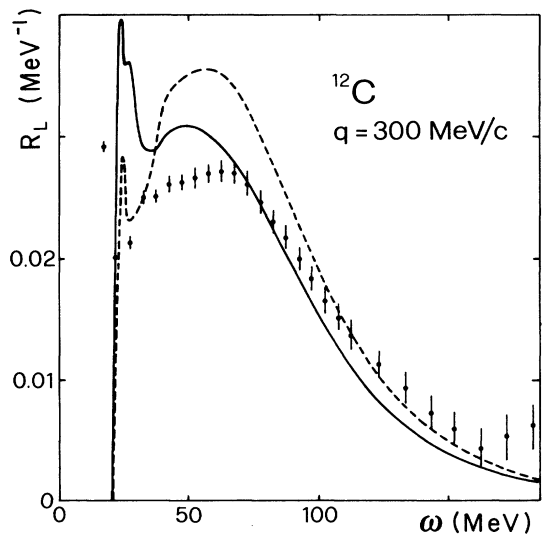

FIG. 11. Same as Fig. 10, but for $q=300$ MeV/c; the discrete isoscalar octupole level is not shown explicitly.

$L=3$ excitations (see Ref. 3). We have performed such calculations and found results in qualitative agreement with the old discrete RPA calculations of Gillet and collaborators,[17] both for the energy and the form factor of such states. While for photoabsorption the TDA and RPA give rather similar results, as shown in Fig. 7, for the isoscalar collective levels the RPA state is shifted further down in energy and is more enhanced than the TDA state. A simple interpretation of these results is offered by the schematic model.[18]

As an example of a low-lying collective state, in Fig. 10 we show explicitly the contribution of the isoscalar $L=3$ level to the longitudinal response at $q=200$ MeV/c. This state is placed by the residual interaction very near to the experimental excitation energy of 9.6 MeV (a recoil energy of about 2 MeV should be subtracted from ω). In this respect our result differs from that of Ref. 17 since in that calculation the octupole state could not be shifted below 12 MeV excitation energy. Being highly collective, this state, together with the low-lying quadrupole state, accounts for a non-negligible amount of the longitudinal cross section.

V. SUMMARY

We have performed a calculation of both the longitudinal response function and the total photoabsorption cross section of ^{12}C. The calculation is based on a Green's function approach. We have generalized to the RPA the doorway-state method developed in Ref. 3 for the TDA. Thus we have been able to include in our calculations the effect of many-particle many-hole excitations, both at the level of self-energy insertions (through a complex phenomenological optical potential for both particles and holes) and at the level of particle-hole rescattering (through the advanced part of the particle-hole Green's function). Apart from some minor formal complications, the generalization of the doorway-state method to the RPA is straightforward. The resulting continued-fraction expansion for the polarization propagator provides a powerful algorithm for solving the RPA integral equation.

Our calculations of the longitudinal response function show that RPA correlations do not resolve the discrepancy between the single-particle model and experiment in the quasielastic region for $q=300$–500 MeV/c. The impossibility of explaining the missing strength problem as an effect of particle-hole rescattering was already pointed out in Ref. 3 on the basis of our TDA calculation. The disagreement between theory and experiment is even more pronounced in the RPA. We have shown above that this failure of both the TDA and RPA lies in the fact that the integrated strength (sum rule) is essentially preserved in both approximations (NEWSR in the TDA and EWSR in the RPA). Thus, as pointed out already in Ref. 3, the solution of the problem cannot lay in the use of a more sophisticated residual interaction, as long as this is kept real. However, a complex residual interaction, such as would be suggested, for example, by the effect of 1p-1h to 2p-2h coupling on the residual particle-hole interaction,[19] could change somewhat the calculated response.

In the photoabsorption calculation, particle-hole rescat-

tering is essential for shifting the main $1p_{3/2}\rightarrow d_{5/2}$ transition strength up in energy to the experimental maximum. However, other processes must be taken into account in order to reproduce the strength and the shape of the isovector dipole response. The strength of the main peak at 23 MeV is very sensitive to the surface part of the imaginary optical potential. Also, the phenomenological width of the $1s_{1/2}$-hole energies must be included in order to smear out an additional peak which would otherwise show up both in photoabsorption and electron scattering. By taking into account all these effects, we can get a very reasonable fit of both the photoabsorption cross section and the longitudinal electron scattering response function at 200 MeV/c momentum transfer.

In view of the success of our theory at low momentum transfer, the disagreement arising for $q \geq 300$ MeV/c is particularly puzzling. It might be due to the increasing importance, with momentum transfer, of some effect which has not been included in our calculations.

ACKNOWLEDGMENTS

We wish to express our thanks to Prof. F. Lenz for his hospitality at the Schweizerisches Institut für Nuklearforschung and for many helpful suggestions. This work was partially supported by the Istituto Nazionale di Fisica Nucleare (Italy), Sezione di Firenze, and by the Ministero Publica Istruzione, Italy. One of us (F.A.B.) was supported by FONDECYT, Chile, Project No. 1242.

APPENDIX

Here we give the detailed expressions of the quantities needed to calculate the continued-fraction expansion of the partial-wave decomposed RPA polarization propagator. We assume that the external operator $O(q)$ is of the form given in Eqs. (C1) of Ref. 3. Since these are intrinsic operators, the single-particle Green's functions should be evaluated at the intrinsic excitation energy ϵ, which differs from the electron energy loss ω by the c.m. recoil energy (see Ref. 3 for details):

$$\epsilon=\omega-q^2/(2Am) .$$

The partial-wave decomposition of the doorway states analogous to Eqs. (3.16) of Ref. 3 now becomes

$$N^0\langle D^0_{\pm} \mid \mathbf{r}_2\rangle=4\pi\sum_{LM}(-i)^L Y_{LM}(\hat{\mathbf{q}})N^0_L\langle (D^0_{\pm})_{LM} \mid \mathbf{r}_2\rangle , \tag{A1a}$$

$$\tilde{N}^0\langle \mathbf{r}_2 \mid \tilde{D}^0_{\pm}\rangle=4\pi\sum_{LM}(i)^L Y_{LM}(\hat{\mathbf{q}})\tilde{N}^0_L\langle \mathbf{r}_2 \mid (\tilde{D}^0_{\pm})_{LM}\rangle , \tag{A1b}$$

with

$$N^0_L\langle (D^0_{+})_{LM} \mid \mathbf{r}_2\rangle=\sum_i\sum_{j_\alpha l_\alpha}\langle \tau_i \mid a_L(2)\frac{u_i(r_2)}{r_2}[X^{LM}_{\alpha i}(\hat{\mathbf{r}}_2)]^{\dagger}\langle i^{-1}\mid , \tag{A2a}$$

$$N^0_L\langle (D^0_{-})_{LM} \mid \mathbf{r}_2\rangle=\sum_i\sum_{j_\alpha l_\alpha}a_L(2)\mid \tau_i\rangle\frac{u_i(r_2)}{r_2}(-)^M[X^{L-M}_{\alpha i}(\hat{\mathbf{r}}_2)]\mid i^{-1}\rangle , \tag{A2b}$$

and

$$\tilde{N}^0_L\langle \mathbf{r}_2 \mid (\tilde{D}^0_{+})_{LM}\rangle=\sum_i\sum_{j_\alpha l_\alpha}\mid i^{-1}\rangle\int_0^\infty dr_1\frac{1}{r_2}g^{j_\alpha l_\alpha}(r_2,r_1,\epsilon- \mid \epsilon_i \mid)a_L(1)u_i(r_1)\mid \tau_i\rangle[X^{LM}_{\alpha i}(\hat{\mathbf{r}}_1)] , \tag{A3a}$$

$$\tilde{N}^0_L\langle \mathbf{r}_2 \mid (\tilde{D}^0_{-})_{LM}\rangle=\sum_i\sum_{j_\alpha l_\alpha}\langle i^{-1}\mid\langle \tau_i \mid \int_0^\infty dr_1 u_i(r_1)a_L(1)\frac{1}{r_2}g^{j_\alpha l_\alpha}(r_1,r_2,-\epsilon- \mid \epsilon_i \mid)(-)^M[X^{L-M}_{\alpha i}(\hat{\mathbf{r}}_2)]^{\dagger} . \tag{A3b}$$

The new quantities appearing in these equations have been defined in Ref. 3.

Now we take the projection of the various components of the operator $\hat{\Omega}^0$ on the particle angular momentum and isospin eigenstates. We define [cf. Eqs. (C2) of Ref. 3]

$$W^{ij}_{\beta\alpha}(r_2,r_4)=\int d\hat{\mathbf{r}}_2 d\hat{\mathbf{r}}_4[\mathcal{Y}^{m_\beta}_{j_\beta l_\beta}(\hat{\mathbf{r}}_2)]^{\dagger}\langle j^{-1}\mid\langle \tau_\beta\mid\langle \mathbf{r}_2\mid \hat{W}\mid \mathbf{r}_4\rangle\mid\tau_\alpha\rangle\mid i^{-1}\rangle\mathcal{Y}^{m_\alpha}_{j_\alpha l_\alpha}(\hat{\mathbf{r}}_4) \tag{A4a}$$

and

$$X^{ij}_{\beta\alpha}(r_2,r_4)=\int d\hat{\mathbf{r}}_2 d\hat{\mathbf{r}}_4[\mathcal{Y}^{m_\beta}_{j_\beta l_\beta}(\hat{\mathbf{r}}_2)]^{\dagger}[\mathcal{Y}^{m_\alpha}_{j_\alpha l_\alpha}(\hat{\mathbf{r}}_4)]^{\dagger}\langle j^{-1}\mid\langle \tau_\beta\tau_\alpha\mid\langle \mathbf{r}_2\mid \hat{X}\mid \mathbf{r}_4\rangle\mid i^{-1}\rangle , \tag{A4b}$$

$$Y^{ij}_{\beta\alpha}(r_2,r_4)=\int d\hat{\mathbf{r}}_2 d\hat{\mathbf{r}}_4\langle j^{-1}\mid\langle \mathbf{r}_2\mid \hat{Y}\mid \mathbf{r}_4\rangle\mid\tau_\beta\tau_\alpha\rangle\mid i^{-1}\rangle\mathcal{Y}^{m_\beta}_{j_\beta l_\beta}(\hat{\mathbf{r}}_2)\mathcal{Y}^{m_\alpha}_{j_\alpha l_\alpha}(\hat{\mathbf{r}}_4) , \tag{A4c}$$

$$Z^{ij}_{\beta\alpha}(r_2,r_4)=\int d\hat{\mathbf{r}}_2 d\hat{\mathbf{r}}_4[\mathcal{Y}^{m_\alpha}_{j_\alpha l_\alpha}(\hat{\mathbf{r}}_4)]^{\dagger}\langle j^{-1}\mid\langle \tau_\alpha\mid\langle \mathbf{r}_2\mid \hat{Z}\mid \mathbf{r}_4\rangle\mid i^{-1}\rangle\mid\tau_\beta\rangle\mathcal{Y}^{m_\beta}_{j_\beta l_\beta}(\hat{\mathbf{r}}_2) . \tag{A4d}$$

Eventually, we will be interested in the linear combinations

$$\sum_{m_j m_\beta} R^{LM}_{\beta j} W^{ji}_{\beta\alpha}(r_2,r_4)=\frac{4\pi}{r_2 r_4}\int_0^\infty dr_3 g^{j_\beta l_\beta}(r_2,r_3,\epsilon-|\epsilon_j|)u_j(r_3)u_i(r_4)v_L(r_3,r_4)$$
$$\times\{\delta_{\tau_\alpha\tau_i}\delta_{\tau_\beta\tau_j}[a_0+\tfrac{1}{2}a_1F_L(\beta,j,\alpha,i)]+\delta_{\tau_\alpha\tau_\beta}\delta_{\tau_i\tau_j}[a_2+\tfrac{1}{2}a_3F_L(\beta,j,\alpha,i)]\}A_2(L,\beta,j)R^{LM}_{\alpha i}$$
$$-\frac{4\pi}{r_2 r_4}g^{j_\beta l_\beta}(r_2,r_4,\epsilon-|\epsilon_j|)$$
$$\times\int_0^\infty dr_3 u_j(r_3)u_i(r_3)\sum_l v_l(r_3,r_4)\{\delta_{\tau_\alpha\tau_\beta}\delta_{\tau_i\tau_j}[a_0A_3(L,l,\beta,j,\alpha,i)+a_1A_4(L,l,\beta,j,\alpha,i)]$$
$$+\delta_{\tau_\alpha\tau_i}\delta_{\tau_\beta\tau_j}[a_2A_3(L,l,\beta,j,\alpha,i)+a_3A_4(L,l,\beta,j,\alpha,i)]\}R^{LM}_{\alpha i}\ , \tag{A5a}$$

$$\sum_{m_j m_\beta} R^{LM}_{\beta j} X^{ji}_{\beta\alpha}(r_2,r_4)=\frac{4\pi}{r_2 r_4}\int_0^\infty dr_3 g^{j_\beta l_\beta}(r_2,r_3,\epsilon-|\epsilon_j|)v_L(r_3,r_4)u_j(r_3)u_i(r_4)$$
$$\times\{\delta_{\tau_\alpha\tau_i}\delta_{\tau_\beta\tau_j}[a_0+\tfrac{1}{2}a_1F_L(\beta,j,i,\alpha)]+\delta_{\tau_i\tau_\beta}\delta_{\tau_\alpha\tau_j}[a_2+\tfrac{1}{2}a_3F_L(\beta,j,i,\alpha)]\}A_2(L,\beta,j)R^{LM}_{i\alpha}$$
$$-\frac{4\pi}{r_2 r_4}g^{j_\beta l_\beta}(r_2,r_4,\epsilon-|\epsilon_j|)$$
$$\times\int_0^\infty dr_3 u_j(r_3)u_i(r_3)\sum_l v_l(r_3,r_4)\{\delta_{\tau_\alpha\tau_j}\delta_{\tau_i\tau_\beta}[a_0A_3(L,l,j,\beta,\alpha,i)+a_1A_4(L,l,j,\beta,\alpha,i)]$$
$$+\delta_{\tau_\alpha\tau_i}\delta_{\tau_\beta\tau_j}[a_2A_3(L,l,j,\beta,\alpha,i)+a_3A_4(L,l,j,\beta,\alpha,i)]\}R^{LM}_{i\alpha}\ , \tag{A5b}$$

$$\sum_{m_j m_\beta} R^{LM}_{j\beta} Y^{ji}_{\beta\alpha}(r_2,r_4)=\frac{4\pi}{r_2 r_4}\int_0^\infty dr_3 u_j(r_3)u_i(r_4)v_L(r_3,r_4)g^{j_\beta l_\beta}(r_3,r_2,-\epsilon-|\epsilon_j|)$$
$$\times\{\delta_{\tau_\alpha\tau_i}\delta_{\tau_\beta\tau_j}[a_0^*+\tfrac{1}{2}a_1^*F_L(\beta,j,i,\alpha)]+\delta_{\tau_i\tau_\beta}\delta_{\tau_\alpha\tau_j}[a_2^*+\tfrac{1}{2}a_3^*F_L(\beta,j,i,\alpha)]\}A_2(L,\beta,j)R^{LM}_{\alpha i}$$
$$-\frac{4\pi}{r_2 r_4}\int_0^\infty dr_3 u_j(r_4)u_i(r_3)\sum_l v_l(r_3,r_4)g^{j_\beta l_\beta}(r_3,r_2,-\epsilon-|\epsilon_j|)$$
$$\times\{\delta_{\tau_\alpha\tau_j}\delta_{\tau_i\tau_\beta}[a_0^*A_3(L,l,j,\beta,\alpha,i)+a_1^*A_4(L,l,j,\beta,\alpha,i)]$$
$$+\delta_{\tau_\alpha\tau_i}\delta_{\tau_\beta\tau_j}[a_2^*A_3(L,l,j,\beta,\alpha,i)+a_3^*A_4(L,l,j,\beta,\alpha,i)]\}R^{LM}_{\alpha i}\ , \tag{A5c}$$

$$\sum_{m_j m_\beta} R^{LM}_{j\beta} Z^{ji}_{\beta\alpha}(r_2,r_4)=\frac{4\pi}{r_2 r_4}\int_0^\infty dr_3 u_j(r_3)v_L(r_3,r_4)g^{j_\beta l_\beta}(r_3,r_2,-\epsilon-|\epsilon_j|)u_i(r_4)$$
$$\times\{\delta_{\tau_\alpha\tau_i}\delta_{\tau_\beta\tau_j}[a_0^*+\tfrac{1}{2}a_1^*F_L(\beta,j,\alpha,i)]+\delta_{\tau_\alpha\tau_\beta}\delta_{\tau_i\tau_j}[a_2^*+\tfrac{1}{2}a_3^*F_L(\beta,j,\alpha,i)]\}A_2(L,\beta,j)R^{LM}_{i\alpha}$$
$$-\frac{4\pi}{r_2 r_4}\int_0^\infty dr_3 u_j(r_3)\sum_l v_l(r_3,r_4)u_i(r_3)g^{j_\beta l_\beta}(r_4,r_2,-\epsilon-|\epsilon_j|)$$
$$\times\{\delta_{\tau_\alpha\tau_\beta}\delta_{\tau_i\tau_j}[a_0^*A_3(L,l,\beta,j,\alpha,i)+a_1^*A_4(L,l,\beta,j,\alpha,i)]$$
$$+\delta_{\tau_\alpha\tau_i}\delta_{\tau_\beta\tau_j}[a_2^*A_3(L,l,\beta,j,\alpha,i)+a_3^*A_4(L,l,\beta,j,\alpha,i)]\}R^{LM}_{i\alpha}\ . \tag{A5d}$$

Equation (A5a) is the same as Eqs. (C3) of Ref 3. We have rewritten it here in order to make the comparison with the additional RPA terms [(A5b)–(A5d)] easier. The coefficients A_2, A_3, etc. have been defined in Ref. 3. Note the reversed order of some indexes in Eqs. (A5b)–(A5d) with respect to the corresponding ones in Eq. (A5a). This has the consequence that the angular momentum selection rules can be different in the added RPA terms. For example the sum over l in the exchange part of $X^{ji}_{\beta\alpha}$ runs over different values than the corresponding sum in the exchange part of $W^{ji}_{\beta\alpha}$.

*Permanent address: Departamento de Fisica, Universidad de Chile, Santiago, Chile.
†Permanent address: Dipartimento di Fisica, Universitá degli Studi di Firenze, Firenze, Italy.

[1]Y. Horikawa, F. Lenz, and N. C. Mukhopadhyay, Phys. Rev. C **22**, 1680 (1980).
[2]P. Barreau *et al.*, Nucl. Phys. **A402**, 515 (1983); Z. E. Meziani *et al.*, Phys. Rev. Lett. **52**, 2130 (1984).
[3]A. Dellafiore, F. Lenz, and F. A. Brieva, Phys. Rev. C **31**, 1088 (1985).
[4]M. Cavinato, D. Drechsel, E. Fein, M. Marangoni, and A. M. Saruis, Nucl. Phys. **A423**, 376 (1984).
[5]U. Stroth, R. Hasse, and P. Schuck, Phys. Lett. **171B**, 339 (1986).
[6]A. L. Fetter and J. D. Walecka, *Quantum Theory of Many-Particle Systems* (McGraw-Hill, New York, 1971).
[7]G. F. Bertsch and S. F. Tsai, Phys. Rep. **18**, 125 (1975).
[8]P. Barreau *et al.*, CEA-N-2334, Commissariat a l'Energie Atomique (France) Report 1983 (unpublished).
[9]V. V. Balashov, S. I. Grishanova, N. M. Kabachnik, V. M. Kulikov, and N. N. Titarenko, Nucl. Phys. **A216**, 574 (1973).
[10]J. Ahrens *et al.*, Nucl. Phys. **A251**, 479 (1975).
[11]C. A. Engelbrecht and H. Fiedeldey, Ann. Phys. (N.Y.) **42**, 262 (1967).
[12]G. F. Bertsch, P. F. Bortignon, and R. A. Broglia, Rev. Mod. Phys. **55**, 287 (1983).
[13]M. Cavinato, M. Marangoni, P. L. Ottaviani, and A. M. Sarius, Nucl. Phys. **A373**, 445 (1982).
[14]D. J. Rowe and S. S. M. Wong, Nucl. Phys. **A153**, 561 (1970).
[15]S. Frullani and J. Mougey, Adv. Nucl. Phys. **14**, 1 (1984).
[16]S. Adachi and N. Van Giai, Phys. Lett. **149B**, 447 (1984).
[17]V. Gillet and A. Melkanoff, Phys. Rev. **133**, B1190 (1964); V. Gillet and N. Vinh Mau, Nucl. Phys. **54**, 321 (1964).
[18]P. Ring and P. Schuck, *The Nuclear Many-Body Problem* (Springer-Verlag, New York, 1980), p. 320.
[19]S. Adachi and S. Yoshida, Nucl. Phys. **A306**, 53 (1978).